BIOCHEMISTRY
including biophysical chemistry & molecular biology

Article

pubs.acs.org/biochemistry

Thermodynamics of Ligand Binding to a Heterogeneous RNA Population in the Malachite Green Aptamer

Joshua E. Sokoloski, Sarah E. Dombrowski,[†] and Philip C. Bevilacqua*

Department of Chemistry, The Pennsylvania State University, University Park, Pennsylvania 16802, United States

Supporting Information

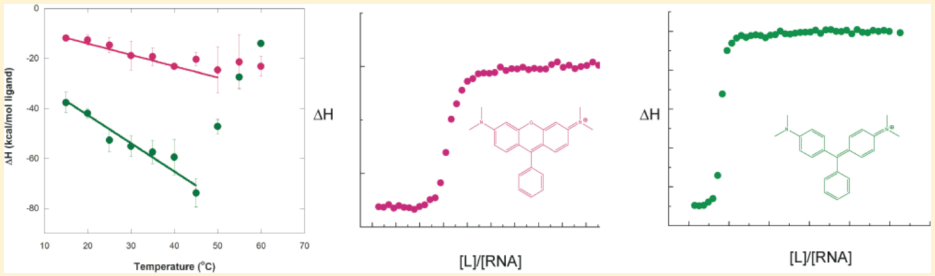

ABSTRACT: The malachite green aptamer binds two closely related ligands, malachite green (MG) and tetramethylrosamine (TMR), with nearly equal affinity. The MG ligand consists of three phenyl rings emanating from a central carbon, while TMR has two of the three rings connected by an ether linkage. The binding pockets for MG and TMR in the aptamer, known from high-resolution structures, differ only in the conformation of a few nucleotides. Herein, we applied isothermal titration calorimetry (ITC) to compare the thermodynamics of binding of MG and TMR to the aptamer. Binding heat capacities were obtained from ITC titrations over the temperature range of 15−60 °C. Two temperature regimes were found for MG binding: one from 15 to 45 °C where MG bound with a large negative heat capacity and an apparent stoichiometry (n) of ∼0.4 and another from 50 to 60 °C where MG bound with a positive heat capacity and an n of ∼1.1. The binding of TMR, on the other hand, revealed only one temperature regime for binding, with a more modest negative heat capacity and an n of ∼1.2. The large difference in heat capacity between the two ligands suggests that significantly more conformational rearrangement occurs upon the binding of MG than that of TMR, which is consistent with differences in solvent accessible surface area calculated for available ligand-bound structures. Lastly, we note that the binding stoichiometry of MG was improved not only by an increase in the temperature but also by a decrease in the concentration of Mg^{2+} or an increase in the time between ITC injections. These studies suggest that binding of a dynamical ligand to a functional RNA requires the RNA itself to have significant dynamics.

Aptamers are RNA molecules obtained via in vitro selection that bind a small molecule or protein.[1−3] RNA aptamers typically have high affinity and specificity for their targets, which has led to them being employed in numerous applications.[4−8] The malachite green aptamer is a 38-nucleotide RNA that was selected to bind the dye malachite green (MG) (Figure 1A,B).[9−11] This aptamer has the unusual feature of binding equally well to its cognate ligand, MG, and a related but noncognate ligand, tetramethylrosamine (TMR)[10,12] that possesses an ether linkage between the two dimethylamino-containing phenyl rings (Figure 1C). Rigidity conferred by this connection has been suggested to lower the conformational entropy penalty for binding.[11,12]

There are two high-resolution structures available for the MG aptamer: an X-ray crystal structure bound to TMR at 2.8 Å resolution (Figure 1D)[10] and an NMR solution structure bound to MG (Figure 1C).[11] Both complexes have similar binding pockets in which the ligand stacks between the G8:C28 base pair and the C7:G24:A31:G29 base quadruple, with C10:G23:A27 and U11:A22:A26 base triples providing key structural portions of the binding cavity's shape. These structures also have differences in their binding pocket architecture, especially with regard to *syn* bases (Figure S1 of the Supporting Information).[13] The TMR-bound complex has two *syn* bases in the binding pocket, G24 and A30, while the MG-bound complex has three *syn* bases in the binding pocket, G24, G29, and A31, with A30 in the standard *anti* conformation. Moreover, both of the *syn* bases in the TMR complex are in the full *syn* conformation, while the three *syn* bases in the MG complex are intermediate *syn*.[13] These differences in binding pocket architecture suggest that the RNA structure likely plays a major role in aptamer selectivity.

The binding heat capacity (ΔC_p), obtained by measuring binding enthalpy (ΔH) as a function of temperature, provides a measure of the conformational changes associated with binding and can be expressed in terms of bond formation (ΔH) or conformational rearrangement (ΔS)[14]

Received: October 28, 2011
Revised: December 2, 2011
Published: December 16, 2011

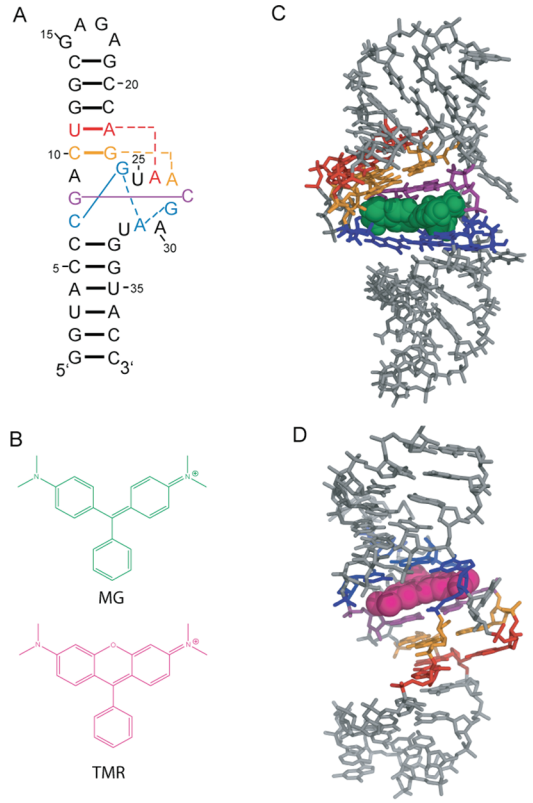

Figure 1. Secondary and tertiary structures of the malachite green aptamer free and bound to MG and TMR. (A) Secondary structure of the aptamer.[11] Key base interactions involved in the binding pocket are colored and correspond with panels C and D. (B) Structures of MG and TMR, which differ only in the presence of an ether linkage in TMR. (C) NMR solution structure of the MG-bound aptamer (PDB entry 1Q8N).[11] MG is colored green. (D) X-ray crystallography structure of the TMR-bound aptamer (PDB entry 1F1T).[10] TMR is colored magneta. Structures were rendered with PyMOL (Schrodinger, Cambridge, MA).

$$\Delta C_{p,\text{binding}} = \left(\frac{\partial \Delta H_{\text{binding}}}{\partial T}\right)_p = T\left(\frac{\partial \Delta S_{\text{binding}}}{\partial T}\right)_p \quad (1)$$

Equation 1 suggests that if binding involves compaction of the RNA that increases in magnitude with temperature then binding should have a large negative ΔC_p.[15] A large negative heat capacity has been associated with formation of RNA structure[16] and with specificity of binding in protein−nucleic acid[17,18] and small molecule−RNA interactions.[19]

In this study, we investigated binding of MG and TMR to the MG aptamer using ITC. We find that the MG aptamer exhibits a negative ΔC_p for interaction with both ligands (for temperatures up to ~45 °C), but that the ΔC_p is significantly larger in magnitude for MG. This observation suggests that larger conformational rearrangement of the RNA occurs upon binding of MG. In addition, the apparent stoichiometry for binding of MG is found to be dependent on temperature, Mg^{2+} concentration, and time, suggesting that the unbound state of the aptamer consists of a heterogeneous population of folds that require significant dynamics to bind the more dynamical ligand.

MATERIALS AND METHODS

RNA Preparation. The MG aptamer was produced by in vitro transcription from a hemiduplex template[20] constructed from the following sequences: T7 promotor + G, 5′ TAA TAC GAC TCA CTA TAG; and aptamer template, 5′ GGT ACC ATT CGT TAC CTG GCT CTC GCC AGT CGG GTA CCT ATA GTG AGT CGT ATT A. Following polyacrylamide gel electrophoresis (PAGE) purification, the band containing the MG aptamer was crushed and soaked in 1× TEN_{250}, and the RNA pellet was obtained via ethanol precipitation. The pellet was dissolved in ITC buffer [10 mM sodium cacodylate (pH 5.8) and 10 mM KCl] and dialyzed against the same buffer for 15−18 h at 4 °C using molecular weight cutoff 1000 membranes (SpectraPor 7, SpectraPor Inc.). This window of time was chosen because shorter periods of time (e.g., 10 h) revealed larger injection heats (data not shown), while longer periods of time might lead to RNA degradation. Buffer conditions for ITC were chosen to be similar to crystallization conditions.[10] Prior to ITC, the aptamer was diluted as needed in the dialysis flow-through buffer and renatured by being heated at 90 °C for 2 min, cooled at room temperature for 1 min, supplemented with $MgCl_2$ from a stock made from solid $MgCl_2$ dissolved in 1× ITC buffer, and incubated at 55 °C for 10 min. Typical final concentrations of Mg^{2+} were 10 mM, although this was lowered in select experiments. RNA concentrations were measured at 90 °C using an ε_{260} of 376300 M^{-1} cm^{-1}, calculated with RNAcalc.[21]

Ligand Preparation. Malachite green oxalate (Sigma Aldrich) and tetramethylrosamine chloride (Invitrogen) were dissolved in the MG aptamer dialysis flow-through buffer, with $MgCl_2$ added from $MgCl_2$ stocks dissolved in 1× ITC buffer prepared as described above. Concentrations of dyes were determined spectrophotometrically using an ε_{617} of 147800 M^{-1} cm^{-1} and an ε_{552} of 52430 M^{-1} cm^{-1} for MG and TMR, respectively, derived from massing a quantity, dissolving it in ITC buffer, and taking an OD reading at the maximal observed wavelength. As a test of purity, MG was recrystallized from the original oxalate salt to a chloride salt using the procedure of Swain and Hedberg.[22] No differences were observed in the calorimetric experiments, indicating that any MG impurities did not affect the data. Care was taken to keep the solutions from light as much as possible, although no photosensitivity was observed.

Isothermal Titration Calorimetry. All ITC experiments were performed on a VP-ITC (MicroCal, Inc., Northampton, MA). Concentrations of the MG aptamer were in the range of 2−4 μM, with the initial ligand concentrations being 12−15 times the initial RNA concentration. Samples were degassed at 35 °C for 10 min prior to being loaded into the instrument. The MG or TMR solutions were injected into the sample cell in 7 or 10 μL increments, with a 5 min period between injections (unless otherwise noted), which was sufficient for the signal to return to baseline. The final five points of each titration were averaged and subtracted from each point in the titration to account for ligand dilution. This method of baseline correction was justified because such injection heats were small and consistent; moreover, the small value of these injection heats confirmed that the RNA and ligand, prepared as described above, were well matched in their buffers. Titration data were integrated and analyzed using Origin (OriginLab Corp., Northampton MA). Errors are reported as the standard error of the mean of multiple trials, typically three or more (see

dx.doi.org/10.1021/bi201642p | Biochemistry 2012, 51, 565−572

Table 1. ITC Data for MG Binding[a]

temp (°C)	no. of trials	apparent stoichiometry	apparent K_d (nM)	$\Delta H°$ (kcal/mol)	$\Delta S°$ (eu)
15	3	0.41 ± 0.03	30 ± 10	−38 ± 4	−100 ± 10
20	3	0.43 ± 0.01	30 ± 10	−42 ± 3	−109 ± 6
25	3	0.40 ± 0.02	50 ± 20	−53 ± 5	−140 ± 10
30	3	0.41 ± 0.02	100 ± 20	−55 ± 4	−150 ± 10
35	2	0.389 ± 0.004	180 ± 70	−57 ± 5	−160 ± 10
40	2	0.345 ± 0.007	300 ± 100	−59 ± 7	−160 ± 20
45	2	0.36 ± 0.07	600 ± 300	−74 ± 6	−200 ± 20
50	2	0.56 ± 0.03	1000 ± 400	−47 ± 3	−120 ± 10
55	3	0.9 ± 0.1	1100 ± 200	−27 ± 4	−60 ± 10
60	1	1.07	2300	−14	−18

[a]All experiments were performed in 10 mM sodium cacodylate (pH 5.8) with 10 mM KCl and 10 mM $MgCl_2$. Errors are the standard error of the mean. Errors in K_d were typically larger than in apparent stoichiometry or enthalpy because of the increased sensitivity to scatter in the transition region of the ITC curve.

Table 2. ITC Data for TMR Binding[a]

temp (°C)	no. of trials	apparent stoichiometry	apparent K_d (nM)	$\Delta H°$ (kcal/mol)	$\Delta S°$ (eu)
15	3	1.1 ± 0.2	29 ± 6	−11.9 ± 0.5	−7 ± 2
20	2	1.4 ± 0.2	40 ± 20	−13 ± 2	−9 ± 6
25	2	1.4 ± 0.2	60 ± 30	−15 ± 2	−16 ± 8
30	8	1.2 ± 0.1	70 ± 20	−19 ± 2	−29 ± 6
35	4	1.2 ± 0.1	90 ± 10	−19 ± 2	−30 ± 6
40	2	1.0 ± 0.3	400 ± 200	−23.2 ± 0.2	−44 ± 2
45	3	1.0 ± 0.2	500 ± 200	−20 ± 2	−35 ± 5
50	3	1.1 ± 0.2	700 ± 200	−25 ± 5	−50 ± 20
55	3	1.3 ± 0.3	600 ± 300	−21 ± 6	−40 ± 20
60	2	1.26 ± 0.06	1300 ± 100	−23 ± 3	−43 ± 9

[a]All experiments were performed in 10 mM sodium cacodylate (pH 5.8) with 10 mM KCl and 10 mM $MgCl_2$. Errors are the standard errors of the mean. Errors in K_d were typically larger than in apparent stoichiometry or enthalpy because of the increased sensitivity to scatter in the transition region of the ITC curve.

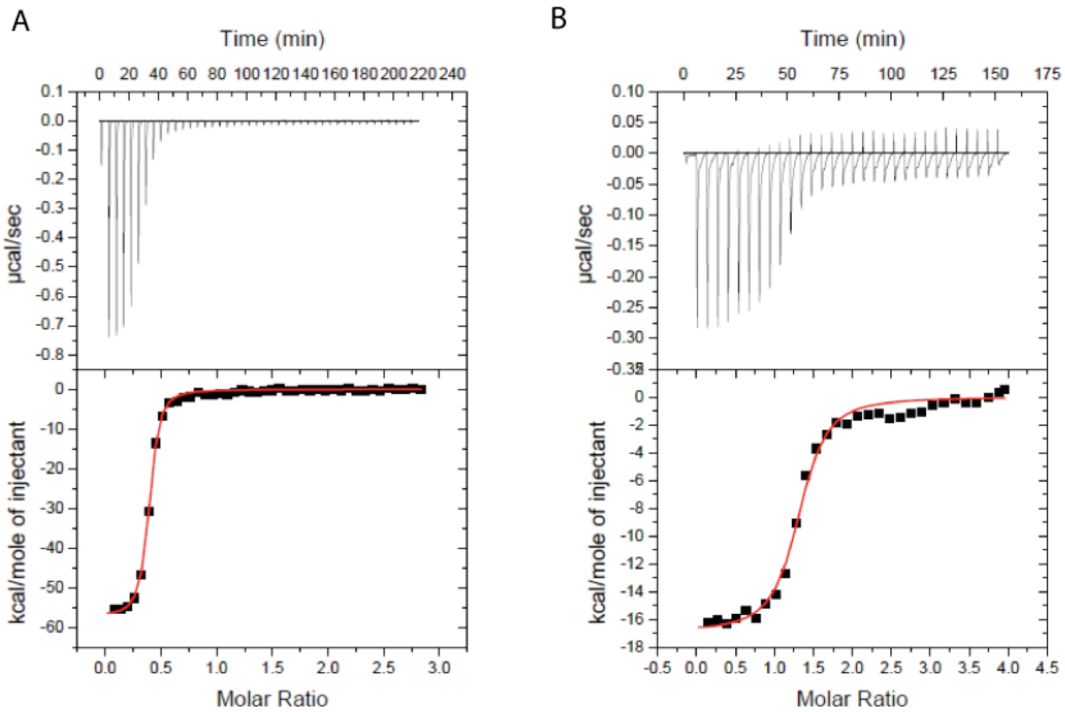

Figure 2. ITC data for ligand binding to the MG aptamer: (A) 53.9 μM MG titrated into 4.36 μM MG aptamer at 25 °C and (B) 56.6 μM TMR titrated into 3.29 μM MG aptamer at 25 °C. Note the greater dynamic range of heat for MG, which reflects its binding with much greater exothermicity. The *x*-axis is the molar ratio of ligand added to total RNA. Binding thermodynamic parameters are listed in Tables 1 and 2.

dx.doi.org/10.1021/bi201642p | *Biochemistry* 2012, 51, 565−572

tables for the actual number of trials). Heat capacities were obtained by fitting temperature-dependent enthalpy values to the following equation, using ΔH_{25} as a reference enthalpy

$$\Delta H(T) = \Delta C_p(T - 25°\text{C}) + \Delta H_{25} \quad (2)$$

Fits were by linear least-squares with weighting to the standard error of the mean for the enthalpy.

Solvent Accessible Surface Area (ASA) Calculation. The solvent accessible surface area (ASA) of the MG-bound and TMR-bound structures was calculated using the web-based program GETAREA[23] with a probe size of 1.4 Å, which approximates the radius of a water molecule.[24] Each RNA–ligand structure contained the same number of nucleotides, allowing direct comparison of ΔASA values for the two structures. Water and metal ions were removed prior to calculation, but ligands were left to properly represent the final bound state.

Thermal Denaturation Monitored by UV Absorption. All thermal denaturation experiments were conducted in a Gilford Response spectrophotometer using 0.1, 0.5, or 1 cm pathlength quartz cuvettes, which allowed different concentrations of RNA to be used. Samples were prepared like ITC samples, with the exclusion of the 55 °C renaturation step for samples studied in the absence of divalent ions. Absorbance at 260 nm was monitored from 20 to 95 °C, with data collected every 0.5 °C. Solutions containing Mg^{2+} were melted once, while solutions without Mg^{2+} were melted multiple times and gave superimposable heating and cooling curves. Melting temperatures were determined from the maximum of a first-derivative plot with five-point smoothing. Data are the average of three melting curves.

UV Cross-Linking of 4-Thiouridine-Containing RNA. Experiments generally followed the protocol of McGraw and co-workers.[25] Briefly, 4-thiouridine triphosphate (TriLink Biotechnolgies) in a 1:1 mixture with UTP was incorporated into the aptamer via in vitro transcription, which also contained [α-^{32}P]GTP. The transcription reaction mixture was purified via a Sephadex G20 spin column and mixed with 10× ITC buffer and water, yielding the same concentrations as in ITC. Samples were renatured according to the ITC sample procedure, and ligands were added afterward. While resting on an ice-chilled aluminum block acting as a heat sink, 20 μL drops of the sample on Parafilm were irradiated with 312 nm light from a UV-B bulb for 30 min. Samples were then mixed with a 2× EDTA formamide loading buffer and fractionated via 10% PAGE under denaturing conditions.

RESULTS

Ligand Binding to the MG Aptamer Is Enthalpically Driven, with an Observed Stoichiometry of <1. We begin by considering ligand binding at our reference temperature of 25 °C. As described below, this temperature is centered in the low-temperature binding regime for MG. At 25 °C, MG and TMR bound the MG aptamer with nearly equal affinity [apparent K_d values of 50 ± 20 and 60 ± 30 nM, respectively (Tables 1 and 2)], but with very different thermodynamic origins (Figure 2). At this temperature, MG bound with a large favorable enthalpy (−53 ± 5 kcal/mol) and a large penalizing entropy (−140 ± 10 eu), while TMR bound with a modest enthalpy (−15 ± 2 kcal/mol) and a less penalizing entropy (−16 ± 8 eu). These trends in $\Delta H°$ and $\Delta S°$ are consistent with general expectations of enthalpy–entropy compensation for ligand binding to a macromolecule.[26]

The observed binding stoichiometry differs significantly between the two ligands. At 25 °C, TMR binds with an apparent stoichiometry near 1:1 (n = 1.4 ± 0.2) while MG binds with a significantly smaller apparent stoichiometry (n = 0.40 ± 0.02). Moreover, these values were consistent across multiple independent trials (Tables 1 and 2). It should be noted that the observed stoichiometry does not affect the enthalpy values. $\Delta H°$ is calculated as kilocalories per mole of ligand injected, all of which has plenty of RNA to which to bind in the initial injections. Indeed, the integrated heat for the early injections (Figure 2A, bottom panels) is approximately equal to the ΔH calculated from model fitting. In addition, the value of n does not affect the apparent K_d value, as the dissociation constant is dependent upon only the slope and curvature of the transition region.

Temperature-Dependent Enthalpy Changes for MG Binding Reveal Two Temperature Regimes. We next examined ligand binding at different temperatures. To elucidate the heat capacity for ligand binding, ITC measurements were taken over a wide temperature range, 15–60 °C. Tables 1 and 2 give the data for these measurements, while Figure 3 provides plots of $\Delta H°$ versus temperature. The heat capacity plot in Figure 3 reveals that MG binding has two distinct temperature regimes: one at the lower temperatures of 15–45 °C, wherein binding becomes increasingly exothermic with temperature (i.e., negative ΔC_p value), and the other in the range of 45–60

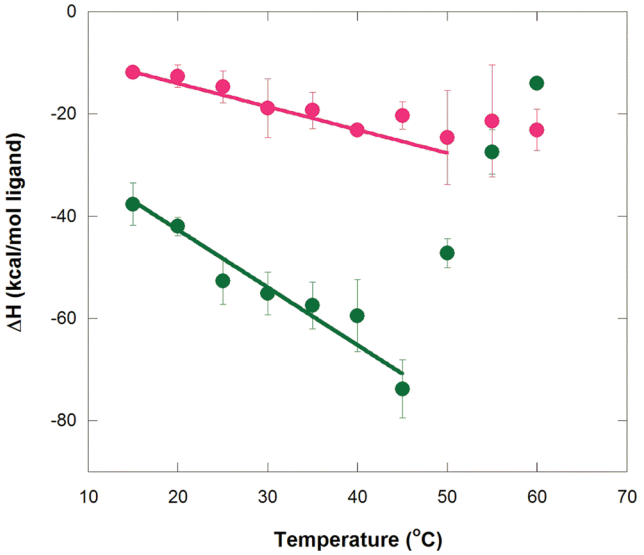

Figure 3. Temperature dependence of enthalpy for binding of the aptamer to MG and TMR. Circles represent average $\Delta H°$ values at a given temperature for MG (green) and TMR (magenta). Error bars are the standard error of the mean. Weighted linear regression of MG binding over the temperature range of 15–45 °C gives a $\Delta H(T)$ of −1.13 kcal mol^{-1} °C^{-1} (T − 25 °C) − 48.3 kcal/mol (R^2 = 0.95), while that for TMR binding over the range of 15–50 °C gives a $\Delta H(T)$ of −0.45 kcal mol^{-1} °C^{-1} (T − 25 °C) − 16.3 kcal/mol (R^2 = 0.97). These plots provide ΔC_p values for MG and TMR of −1.13 ± 0.17 and −0.45 ± 0.035 kcal K^{-1} mol^{-1}, respectively. Note that the values of the final term in these fits are similar to the actual enthalpies for MG and TMR measured at 25 °C (provided in Tables 1 and 2), as expected. The buffer consisted of 10 mM sodium cacodylate (pH 5.8), 10 mM KCl, and 10 mM $MgCl_2$.

°C, wherein binding becomes decreasingly exothermic with temperature (i.e., positive ΔC_p value). The TMR ligand, on the other hand, shows essentially one temperature regime, which extends to at least 50 °C, which has a smaller, negative ΔC_p.

Values of the binding ΔC_p's for interaction of the aptamer with MG and TMR were calculated from the linear fit of $\Delta H°$ versus temperature data in the 15−45 °C regime (fits provided in Figure 3). [We did not calculate ΔC_p for the higher-temperature regime because that region likely couples ligand binding with global folding of the aptamer (see Discussion).] As mentioned, both ligands exhibit negative heat capacity in this temperature range, but the ΔC_p for MG binding is ∼2.5-fold larger in magnitude than that for TMR binding, −1.13 and −0.45 kcal mol^{-1} K^{-1}, respectively. These values suggest that binding of MG involves a larger conformational rearrangement of the ligand, the aptamer, or both relative to the binding of TMR. Comparison of apparent K_d values for MG and TMR (Tables 1 and 2, respectively) shows that the binding affinities for the two ligands are nonetheless approximately equal at the low-temperature end of the data, with a slight preference for the noncognate TMR as the temperature increases, which is as expected given the more exothermic ΔH for binding of MG.

Next, we consider the binding entropy. Tables 1 and 2 give the data for these measurements, while Figure 4 provides the

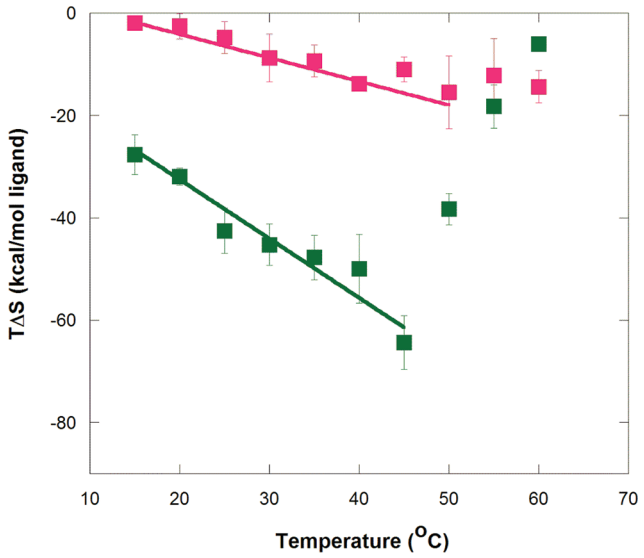

Figure 4. Temperature dependence of entropy for binding of the aptamer to MG and TMR. Squares represent average $T\Delta S°$ values at a given temperature for MG (green) and TMR (magenta). Error bars are from the standard error of the mean. The slope of the fits here is equal to $\Delta C_p + \Delta S$, which is $\sim\Delta C_p$ because ΔS is relatively small. The slope of this plot is not interpreted in detail here because ΔC_p can be directly obtained in Figure 3, and ΔS is available in Tables 1 and 2. Nonetheless, this plot provides the trend of $T\Delta S°$ with temperature. The buffer consisted of 10 mM sodium cacodylate (pH 5.8), 10 mM KCl, and 10 mM $MgCl_2$.

$T\Delta S°$ versus temperature plots for both ligands. Like the enthalpy plots, the entropy plots reveal two temperature regimes. The binding entropy for MG becomes increasingly unfavorable with temperature until approximately 50 °C, at which point it rapidly becomes less unfavorable with temperature (Figure 4). The binding entropy for TMR (Table 2) does not follow this trend; rather, it levels off at high temperatures, akin to the binding enthalpy.

Because heat capacity for biopolymers is often correlated with ΔASA,[17,27,28] we next calculated ΔASA for the TMR-bound structure relative to the MG-bound structure.[23] The total ASA for the TMR complex is 5432 Å^2, while that of the MG complex is 5183 Å^2, providing a ΔASA of ∼250 Å^2. This difference is in line with approximately 1.5 nucleotide less surface area in the MG complex.[29] It should be noted that the two structures were determined under different solution conditions. Specifically, the MG-bound solution structure was determined in the absence of divalent ions, although the authors pointed out that divalent ions had no effect on the NMR spectra.[11,12] With the assumption that both binding interactions in our experiments start with the same initial unbound state (or states), which is reasonable given that the MG aptamer was prepared identically for both ligands, this result indicates that there is greater compaction of the RNA aptamer in the course of binding of MG. This ΔASA thus provides a structural basis for observation of a larger binding heat capacity for MG than for TMR.

The Binding Stoichiometry for MG Is Near Unity in the High-Temperature Regime. Temperature affects not only the binding enthalpy and entropy but also the apparent stoichiometry of binding. The binding stoichiometry for MG increases to ∼1 at 55 and 60 °C, while the stoichiometry for

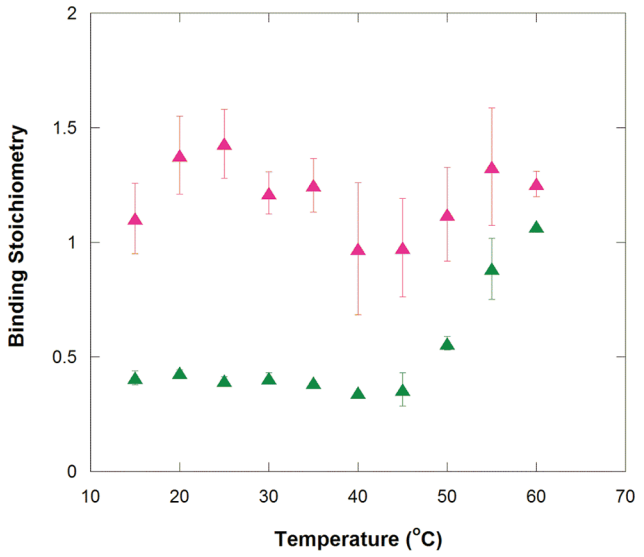

Figure 5. Temperature dependence of the apparent stoichiometry for binding of the aptamer to MG and TMR. Binding stoichiometries for MG (green) and TMR (magenta) binding to the MG aptamer were measured by ITC and are listed in Tables 1 and 2.

TMR remains constant at ∼1.2 across all temperatures (Figure 5).

As mentioned, the ratio of ligand to macromolecule (n) for the MG interaction in the low-temperature binding regime is ∼0.4. This apparent stoichiometry suggests that for every ∼5 aptamers, only ∼2 MG ligands bind, or in other words, ∼60% of all aptamers do not readily accommodate an MG ligand. An alternative case was considered as well, in which MG could bind to a dimer of the aptamer strands, given the near 1:2 observed stoichiometry value. Thermal denaturation monitored by UV spectroscopy and UV cross-linking experiments were performed to assess this possibility. Melts over a ∼20-fold range of aptamer concentrations are provided in Figure S2 of the

dx.doi.org/10.1021/bi201642p | *Biochemistry* 2012, 51, 565−572

Supporting Information and summarized in Table 3. These experiments, in the absence and presence of tertiary structure-promoting divalent metal ions, showed no increase in the melting temperature (T_m) of the aptamer with an increase in RNA concentration, which supports the absence of MG dimerization.

Table 3. Summary of T_m Values for the MG Aptamer[a]

[MG aptamer] (μM) in 0 mM Mg^{2+}	T_m (°C)	[MG aptamer] (μM) in 10 mM Mg^{2+}	T_m (°C)
1.3	59.7 ± 0.3		
2.5	58.5 ± 0.5	2.5	85.2 ± 0.3
5	57 ± 1	5	85.3 ± 0.8
10	58 ± 1	10	85 ± 1
20	57 ± 1	18	84.7 ± 0.3

[a]All results are an average of three scans.

As a second way of assessing the possibility of aptamer dimerization, the photoactivatable cross-linker 4-thiouridine triphosphate was incorporated into the aptamer, followed by exposure to 312 nm light and denaturing PAGE. This experiment was performed in an effort to cross-link any dimer species (Figure S3 of the Supporting Information). No slow mobility bands were observed during gel electrophoresis, however, further supporting the absence of dimer formation. Lastly, we note that if the aptamer were dimerizing it would likely have caused TMR's stoichiometry to be fractional as well because the same aptamer was used for both ligands.

We also noted that TMR's binding stoichiometry is slightly higher than unity, with an average value of 1.21 ± 0.05. The possibility that the more planar TMR interacts nonspecifically with RNA, perhaps by intercalating into the base pairs,[30] was tested. We titrated TMR into $tRNA^{phe}$ (Sigma-Aldrich) under conditions identical to those used for the MG aptamer ITC experiments. We chose tRNA because it has a varied combination of secondary and tertiary structure and sequence. As shown in Figure S4 of the Supporting Information, injection heats with tRNA were consistently 1 order of magnitude smaller than those with the MG aptamer and were similar to background injection heats. There is thus no evidence that TMR has nonspecific interactions with RNA.

The Binding Stoichiometry for MG Is Also Improved by Lower Concentrations of Magnesium and Longer Experimental Time Scales. To explore if the improved stoichiometry of the MG aptamer at high temperatures was due to weakened tertiary structure, ITC experiments were repeated in the presence of lower magnesium ion concentrations, which generally weakens RNA tertiary folding.[31] As the divalent metal ion concentration is decreased from 10 to 0.1 mM, the apparent stoichiometry for MG binding improves. At 30 °C, n is 0.41 at 10 mM Mg^{2+}, but 0.55 at 0.5 and 1 mM Mg^{2+} and 0.59−0.60 at 0 and 0.1 mM Mg^{2+} (Table 4). In addition, the binding enthalpy becomes less exothermic as stoichiometry increases, although the binding affinity is not significantly impaired until all divalent ions are removed from the system. We note that a similar trend was found with higher temperatures: binding enthalpy became significantly less exothermic as stoichiometry increased upon going from 50 to 60 °C (Table 1). Increasing the monovalent concentration from 10 to 100 mM KCl or changing the pH from 5.8 to 6.5 did not affect the n = 0.4 result for MG−aptamer interaction (data not shown). The association of apparent stoichiometry

Table 4. ITC Data for MG Binding as a Function of $MgCl_2$ Concentration[a]

[$MgCl_2$] (mM)	apparent stoichiometry	apparent K_d (nM)	$\Delta H°$ (kcal/mol)
0	0.59	1600	−26
0.1	0.60	130	−40
0.5	0.55	93	−42
1	0.55	150	−48
10	0.41 ± 0.02	100 ± 20	−55 ± 4

[a]All experiments were performed in 10 mM sodium cacodylate (pH 5.8) with 10 mM KCl. Experiments were conducted at 30 °C, which was chosen because it is in the center of the lower-temperature regime.

improvement with lowering of the Mg^{2+} concentration but not the ionic strength in general is suggestive of a role of the unbound state's tertiary structure in affecting the ability of the ligand to bind. Indeed, Dieckmann and co-workers pointed out that the structure of the unbound MG aptamer in the absence of divalent ions has almost no base pairing in the binding pocket, consistent with the lack of tertiary structure under these conditions.[11] These observations suggest the presence of enhanced intramolecular dynamics in the absence of divalent ions.

Observation that both higher temperatures and lower Mg^{2+} concentrations improved the stoichiometry of MG binding suggested that RNA tertiary structure may need to melt prior to MG binding. We reasoned that such a structural transition may be under kinetic control as well. With all titrations for MG and TMR, the injection peaks returned to baseline within 3 min, well within the 5 min injection spacing parameter for the titration. Despite this, we tested the effect of lengthening the time between injections.

Remarkably, increasing the time between the injections improved the MG−aptamer interaction stoichiometry, with the most significant effects occurring in the high-temperature binding regime. Increasing injection spacings from 5 to 25 min had a slight effect on the stoichiometry at 25 °C, improving n from 0.40 to 0.48. However, increasing the injection spacings from 5 to 25 min at 50 °C increased the apparent stoichiometry from 0.56 to 0.85. This result is in line with 50 °C being the transition temperature between the two binding regimes (Figure 3) and thus with longer times improving access to a buried active site.

Notably, this improvement in the apparent stoichiometry did not lead to any observable signal in the ITC injections (Figure S5 of the Supporting Information). In fact, we switched the feedback mode on the VP-ITC instrument from high feedback (i.e., standard mode) to either low feedback or passive mode (i.e., no feedback), as recommended by the manufacturer for detecting any heats associated with slow thermal processes; however, no differences were found, indicating that any net heat associated with this very slow process is below the detection level of the instrument (Figure S5 of the Supporting Information). The molecular basis for the absence of observable heat during the longer injection times is unclear but could reflect the relatively slow rate of binding during this time or a thermoneutral process in which bond breaking and making are roughly balanced.

DISCUSSION

The malachite green aptamer has a complex thermodynamic profile with regard to ligand binding. It binds two related

ligands, MG and TMR, with similar affinities but different enthalpy and entropy profiles. For both ligands, binding is enthalpically driven with an unfavorable binding entropy, but the relative magnitude of these factors differs dramatically. The aptamer binds MG with ~3-fold greater enthalpy than TMR, but also with a 4−10-fold-greater penalty in entropy. Comparison of ligand structures suggests that at least some of this difference is due to the order imposed on the aromatic rings of MG within the confines of the binding pocket, which does not occur in the case of TMR because it is already fixed in a largely coplanar conformation (see Figure 1).

Comparison of the binding pocket architecture of the two complexes indicates that the MG complex has a larger ΔASA (i.e., more compact) than the TMR complex, by ~250 Å^2. With the assumption that both complexes start from the same initial unbound state and that the different solution conditions of the ligand-bound PDB structures do not affect the interactions between the ligand and the binding pocket (see Results), these structural differences help explain thermodynamic differences. In particular, binding of MG is characterized by an ~2.5-fold larger binding heat capacity (−1.13 kcal mol^{-1} K^{-1}) versus that for TMR (−0.45 kcal mol^{-1} K^{-1}) (Figure 3). The magnitude of heat capacity changes has been correlated to conformational changes in the ligand−macromolecule system for many binding systems,[27] including riboswitch−metabolite and DNA−protein interactions.[17−19]

As we noted, there are two regimes to the temperature dependence of enthalpy and entropy (Figures 3 and 4). To help account for this, we provide a model in Scheme 1. Over

Scheme 1

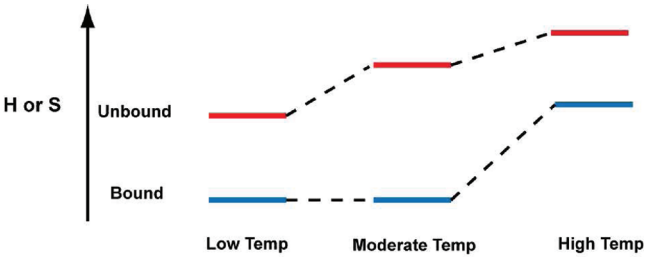

the low-temperature regime of 15−45 °C, the data suggest that the unfolded state becomes more disordered with temperature (negative ΔC_p), while over the high-temperature regime of 45−60 °C, the data suggest that the MG-bound folded state becomes even more disordered with temperature (positive ΔC_p). It is noteworthy that TMR does not show such a steep apparent positive ΔC_p in the high-temperature regime, which may be reflective of TMR not requiring a highly ordered folded state, perhaps because the initial selections were not for TMR.

Heterogeneous Unbound State in the MG Aptamer.

The different binding stoichiometry for MG and TMR, along with the dependence of binding stoichiometry for MG on temperature, divalent ion, and time, provides evidence of a heterogeneous unbound state of the aptamer. Several lines of evidence suggest that the effect of these parameters is on the RNA rather than the ligand: RNA is known to be denatured by higher temperatures and lower divalent ion concentrations, whereas a small molecule ligand is not expected to be strongly sensitive to divalent ion concentration. In addition, RNA can become trapped in stable misfolds, whereas this is unlikely for a small molecule ligand. The observed stoichiometry of ~0.4 for MG binding suggests that the unbound aptamer binding pocket has two or more folds (Scheme 2). The two temperature

Scheme 2

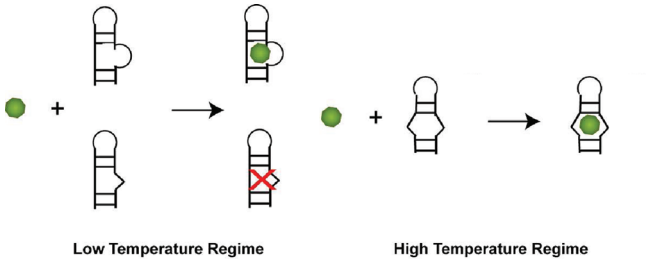

binding regimes observed for MG may be due to partial melting of the unbound binding pocket. In the low-temperature regime, MG can bind only a portion of the aptamer population, and the conformational rearrangement that the RNA and ligand must undergo is extensive, judging by the value of the binding heat capacity. In contrast, TMR can likely access the entirety of the unbound MG aptamer population in this temperature range with fewer structural changes. As the temperature increases (or magnesium concentration decreases) to a point at which the unbound state's tertiary structure has been denatured to a certain extent (Scheme 2-right), all of the MG aptamer molecules are accessible to MG, and it binds with a 1:1 stoichiometry. At the same time, TMR continues to access all of the MG aptamer population at these higher temperatures. We note that a heterogeneous free state has been suggested in the case of the theophylline−RNA complex as well, which was revealed primarily through the Mg^{2+} dependence of the binding kinetics.[32]

The MG Aptamer Is Not Selective for MG or TMR.

Affinities of the MG aptamer for the two ligands, MG and TMR, are approximately equal in the low-temperature regime, and the affinity is only slightly lower for MG in the high-temperature regime. The specificity of the MG aptamer for its cognate ligand is therefore quite poor, at least with respect to TMR. This is especially striking when compared to the case for the theophylline aptamer, which can distinguish caffeine from theophylline by a single methyl group.[33] The nonselective nature of the MG aptamer for a closely related ligand is not surprising, however, as there was no counterselection against TMR,[9] as there was against caffeine in the theophylline aptamer.[33]

A recent thermodynamic study of the MG aptamer explored the specificity of the aptamer as a function of monovalent and divalent metal ion concentrations using ITC.[12] Their results showed that the selectivity for MG over TMR can be tuned via metal ion concentration, with MG binding slightly tighter under low-salt conditions (1 mM NaCl) and equivalently under conditions comparable to those of our study (10 mM $MgCl_2$). These results indicate that tertiary structure stability is a key factor in the function of the MG aptamer, which is in line with our findings for the dependence of binding stoichiometry on temperature and magnesium ions.

In summary, the MG aptamer reveals that dynamics in the RNA, promoted by higher temperatures or lower Mg^{2+} concentrations and captured by waiting long periods of time, are important for binding a dynamic ligand, MG, but not a rigid one, TMR. These results suggest that the binding pocket structure of the MG aptamer consists of a heterogeneous

dx.doi.org/10.1021/bi201642p | Biochemistry 2012, 51, 565−572

population of folds, some of which could be intrinsically disordered, that exclude a dynamic ligand but not a more static one. The ability of the MG aptamer to bind its cognate ligand can be improved by adopting conditions that weaken the tertiary structure of the unbound aptamer. These findings have general ramifications for the ability of functional RNAs to interact with dynamic substrates.

■ ASSOCIATED CONTENT

Supporting Information

Overlay of the TMR and MG binding pockets, UV melting of the MG aptamer, 4-thiouridine triphosphate cross-linking of the MG aptamer, TMR titrated into tRNA measured by ITC, and ITC injection peak morphology. This material is available free of charge via the Internet at http://pubs.acs.org.

■ AUTHOR INFORMATION

Corresponding Author

*Phone: (814) 863-3812. Fax: (814) 865-2927. E-mail: pcb5@psu.edu.

Present Address

[†]School of Pharmacy, University of Pittsburgh, Pittsburgh, PA 15213.

Funding

This work was funded by a National Science Foundation Grant (MCB-0527102) and a National Institutes of Health Predoctoral Fellowship (1F31NS054492-01) to J.E.S.

■ ACKNOWLEDGMENTS

We thank Olke Uhlenbeck and George Makhatadze for helpful discussions.

■ ABBREVIATIONS

MG, malachite green; TMR, tetramethylrosamine; ITC, isothermal titration calorimetry; ASA, accessible surface area; PDB, Protein Data Bank.

■ REFERENCES

(1) Ellington, A. D. (1994) RNA selection. Aptamers achieve the desired recognition. *Curr. Biol. 4*, 427−429.

(2) Joyce, G. F. (1994) In vitro evolution of nucleic acids. *Curr. Opin. Struct. Biol. 4*, 331−336.

(3) Mayer, G. (2009) The chemical biology of aptamers. *Angew. Chem., Int. Ed. 48*, 2672−2689.

(4) Giovannoli, C., Baggiani, C., Anfossi, L., and Giraudi, G. (2008) Aptamers and molecularly imprinted polymers as artificial biomimetic receptors in affinity capillary electrophoresis and electrochromatography. *Electrophoresis 29*, 3349−3365.

(5) Cho, E. J., Lee, J. W., and Ellington, A. D. (2009) Applications of aptamers as sensors. *Annu. Rev. Anal. Chem. 2*, 241−264.

(6) Barbas, A. S., Mi, J., Clary, B. M., and White, R. R. (2010) Aptamer applications for targeted cancer therapy. *Future Oncol. 6*, 1117−1126.

(7) Becker, R. C., Povsic, T., Cohen, M. G., Rusconi, C. P., and Sullenger, B. (2010) Nucleic acid aptamers as antithrombotic agents: Opportunities in extracellular therapeutics. *Thromb. Haemostasis 103*, 586−595.

(8) Khati, M. (2010) The future of aptamers in medicine. *J. Clin. Pathol. 63*, 480−487.

(9) Grate, D., and Wilson, C. (1999) Laser-mediated, site-specific inactivation of RNA transcripts. *Proc. Natl. Acad. Sci. U.S.A. 96*, 6131−6136.

(10) Baugh, C., Grate, D., and Wilson, C. (2000) 2.8 Å crystal structure of the malachite green aptamer. *J. Mol. Biol. 301*, 117−128.

(11) Flinders, J., DeFina, S. C., Brackett, D. M., Baugh, C., Wilson, C., and Dieckmann, T. (2004) Recognition of planar and nonplanar ligands in the malachite green-RNA aptamer complex. *ChemBioChem 5*, 62−72.

(12) Bernard Da Costa, J., and Dieckmann, T. (2011) Entropy and Mg^{2+} control ligand affinity and specificity in the malachite green binding RNA aptamer. *Mol. BioSyst. 7*, 2156−2163.

(13) Sokoloski, J. E., Godfrey, S. A., Dombrowski, S. E., and Bevilacqua, P. C. (2011) Prevalence of syn nucleobases in the active sites of functional RNAs. *RNA 17*, 1775−1787.

(14) Callen, H. B. (1985) *Thermodynamics and an Introduction to Thermostatistics*, 2nd ed., John Wiley and Sons, Inc., New York.

(15) Prabhu, N. V., and Sharp, K. A. (2005) Heat capacity in proteins. *Annu. Rev. Phys. Chem. 56*, 521−548.

(16) Mikulecky, P. J., and Feig, A. L. (2006) Heat capacity changes associated with DNA duplex formation: Salt- and sequence-dependent effects. *Biochemistry 45*, 604−616.

(17) Spolar, R. S., and Record, M. T. Jr. (1994) Coupling of local folding to site-specific binding of proteins to DNA. *Science 263*, 777−784.

(18) Jen-Jacobson, L., Engler, L. E., Ames, J. T., Kurpiewski, M. R., and Grigorescu, A. (2000) Thermodynamic Parameters of Specific and Nonspecific Protein-DNA Binding. *Supramol. Chem. 12*, 143−160.

(19) Gilbert, S. D., Stoddard, C. D., Wise, S. J., and Batey, R. T. (2006) Thermodynamic and kinetic characterization of ligand binding to the purine riboswitch aptamer domain. *J. Mol. Biol. 359*, 754−768.

(20) Bevilacqua, P. C., Brown, T. S., Chadalavada, D., Parente, A. D., and Yajima, R. (2003) in *Kinetic Analysis of Ribozyme Cleavage* (Johnson, K. A., Ed.) pp 49−74, Oxford University Press, Oxford, U.K.

(21) McDowell, J. A. (1995) *RNAcalc*.

(22) Swain, C. G., and Hedberg, K. (1950) The mechanism of oxidation of leuco malachite green by ceric sulfate. *J. Am. Chem. Soc. 72*, 3373−3375.

(23) Rychkov, G., and Petukhov, M. (2007) Joint neighbors approximation of macromolecular solvent accessible surface area. *J. Comput. Chem. 28*, 1974−1989.

(24) Shrake, A., and Rupley, J. A. (1973) Environment and exposure to solvent of protein atoms. Lysozyme and insulin. *J. Mol. Biol. 79*, 351−371.

(25) McGraw, A. P., Mokdad, A., Major, F., Bevilacqua, P. C., and Babitzke, P. (2009) Molecular basis of TRAP-5′SL RNA interaction in the *Bacillus subtilis* trp operon transcription attenuation mechanism. *RNA 15*, 55−66.

(26) Olsson, T. S., Ladbury, J. E., Pitt, W. R., and Williams, M. A. (2011) Extent of enthalpy-entropy compensation in protein-ligand interactions. *Protein Sci. 20*, 1607−1618.

(27) Myers, J. K., Pace, C. N., and Scholtz, J. M. (1995) Denaturant m values and heat capacity changes: Relation to changes in accessible surface areas of protein unfolding. *Protein Sci. 4*, 2138−2148.

(28) Shelton, V. M., Sosnick, T. R., and Pan, T. (1999) Applicability of urea in the thermodynamic analysis of secondary and tertiary RNA folding. *Biochemistry 38*, 16831−16839.

(29) Singh, Y. H., Andrabi, M., Kahali, B., Ghosh, T. C., Mizuguchi, K., Kochetov, A. V., and Ahmad, S. (2010) On nucleotide solvent accessibility in RNA structure. *Gene 463*, 41−48.

(30) Saucier, J. M., Festy, B., and Le Pecq, J. B. (1971) The change of the torsion of the DNA helix caused by intercalation. II. Measurement of the relative change of torsion induced by various intercalating drugs. *Biochimie 53*, 973−980.

(31) Misra, V. K., and Draper, D. E. (1998) On the role of magnesium ions in RNA stability. *Biopolymers 48*, 113−135.

(32) Jucker, F. M., Phillips, R. M., McCallum, S. A., and Pardi, A. (2003) Role of a heterogeneous free state in the formation of a specific RNA-theophylline complex. *Biochemistry 42*, 2560−2567.

(33) Jenison, R. D., Gill, S. C., Pardi, A., and Polisky, B. (1994) High-resolution molecular discrimination by RNA. *Science 263*, 1425−1429.